I&EC research
Industrial & Engineering Chemistry Research

Article

Cite This: Ind. Eng. Chem. Res. 2018, 57, 10226−10233

pubs.acs.org/IECR

Visible-Light-Driven Nitrogen-Doped Carbon Quantum Dots/$CaTiO_3$ Composite Catalyst with Enhanced NO Adsorption for NO Removal

Jiaoyang Wang,[†] Fuman Han,[†] Yongfang Rao,*[,†,§] Tafeng Hu,[§] Yu Huang,*[,‡,§] Jun-ji Cao,[‡,§] and Shun Cheng Lee[∥]

[†]Department of Environmental Science and Engineering, Xi' an Jiaotong University, Xi'an 710049, P. R. China

[‡]Key Laboratory of Aerosol Chemistry and Physics, Institute of Earth Environment, Chinese Academy of Sciences, Xi'an 710075, China

[§]State Key Lab of Loess and Quaternary Geology (SKLLQG), Institute of Earth Environment, Chinese Academy of Sciences, Xi'an 710075, China

[∥]Department of Civil and Environmental Engineering, The Hong Kong Polytechnic University, Hong Kong, China

Supporting Information

ABSTRACT: Nitrogen oxides (NO_x) have attracted extensive concerns as a secondary aerosol precursor in recent years. Solar-induced photocatalytic oxidation is a promising strategy for of NO_x removal nowadays. In this contribution, nitrogen-doped carbon quantum dots (N-CQDs)/$CaTiO_3$ composite was synthesized using a facile hydrothermal process. The incorporation of N-CQDs to $CaTiO_3$ facilitates the transfer of electrons and divorce of photogenerated carriers. NO temperature-programmed desorption (NO-TPD) demonstrated that the presence of N-CQDs was conducive to the NO adsorption in comparison with the pristine $CaTiO_3$. The composite catalyst demonstrated much better photocatalytic performance than $CaTiO_3$ and P25 did in regard to gaseous NO removal and NO_2 selectivity under visible light irradiation. Both $\bullet O_2^-$ and •OH are believed to make a major contribution to NO removal. The role of N-CQDs was unraveled in the photocatalytic reaction of NO elimination over N-CQDs/$CaTiO_3$ samples. This study provides insight into the composite catalyst N-CQDs/$CaTiO_3$ in photocatalytic reactions and applications.

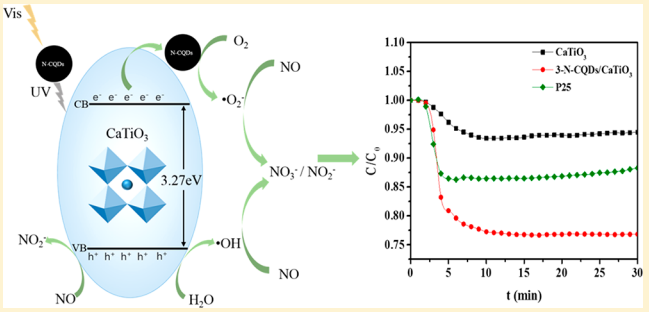

1. INTRODUCTION

In recent decades, the tremendous boost in energy consumption has induced significant NO_x concentration enhancement in the atmosphere in China.[1−3] Nitrogen oxides (NO_x) were reported to be germane to haze events which have received extensive concerns as a secondary aerosol precursor.[4−6] Therefore, the diminution of NO_x concentration is pressing in the atmosphere. Typical deNO_x technologies such as three-way catalysis and selective catalytic reduction entail high temperature and reductants, rendering the elimination of NO_x economically unfeasible at parts per billion (ppb) level in the air.[7−9]

Solar-driven photocatalysis is an attractive alternative for NO_x removal at ppb level.[10−12] Photocatalytic oxidation can convert NO to nitrate, while the generation of uninvited NO_2 may also be expected. Therefore, both high removal efficiency of NO and selectivity toward the formation of nitrate are equally crucial.

In recent years, perovskite-type oxides have gained increasing attention as functional materials because of its inimitable physical and chemical properties.[13−16] The typical structural formula of perovskite-type oxides is ABO_3, in which A indicates a rare or alkaline earth metal and B is occupied by a transition metal. Moreover, titanate perovskites of the type ABO_3 (A = Ca, Sr, Ba, etc.) with high photo and thermal stability are reported as one of the promising materials for photocatalytic processes.[17] Among titanate perovskite-type oxides, $CaTiO_3$ with appropriate conduction band (CB) and valence band (VB) position, has attracted growing attention in the last decades.[18−20] Unfortunately, its high band gap energy (3.5 eV) confines its practical application.[21] In order to effectively utilize solar energy, efforts such as metal doping have been devoted to extend the optical response of $CaTiO_3$ into the visible spectral range.[22] Unfortunately, metal doping may change the band structure of $CaTiO_3$, leading to the variation of the potential of CB and VB, which may not be encouraging for the generation of hydroxyl or superoxide radical. The introduction of quantum dots can offer a

Received: April 21, 2018
Revised: July 20, 2018
Accepted: July 20, 2018
Published: July 20, 2018

DOI: 10.1021/acs.iecr.8b01731
Ind. Eng. Chem. Res. 2018, 57, 10226−10233

possibility to extend the photo response of $CaTiO_3$ into the visible light range without changing its band structure.

Carbon quantum dots (CQDs), a new type of carbon nanomaterial sized smaller than 10 nm, have attracted increasing attention in the photocatalysis realm due to their excellent optical properties, chemical inertness, eco-friendliness, upconversion photoluminescence, and conjugated π structure which allows them to be electron transporters and acceptors.[23−28] However, the CQDs usually show low flurescence quantum yields.[29] Nitrogen doping can lower the work function, encourage charge delocalization, and efficiently promote the electron-transfer capability of CQDs.[30,31] It was also reported that nitrogen doping could increase flurescence quantum yields of CQDs.[29] Owing to their photochemical properties, electrocatalytic activity, biocompatibility, and ability to reduce the work function of CQDs, the N-CQDs showed much better performance than CQDs.[32−34] Zhang et al.[31] reported that N-CQDs/TiO_2 composites have a visible light activity that is two times higher than that of P25, and Wei et al.[35] thought that the activity of TiO_2 for hydrogen evolution under solar sunlight can be enhanced with the addition of N-CQD.

This work presents a N-CQDs/$CaTiO_3$ composite prepared by a simple hydrothermal method. Comprehensive characterizations of the as-prepared catalysts were conducted. We illuminated the roles of N-CQDs in the enhanced photocatalytic activity of N-CQDs/$CaTiO_3$ and proposed the possible photocatalytic mechanisms. It is the first time for N-CQDs/$CaTiO_3$ composites to be used in the photocatalytic removal of NO_x.

2. EXPERIMENTAL SECTION

2.1. Preparation of N-CQDs. A simple hydrothermal method was applied to prepare N-CQDs. Briefly, 3 g of citric acid monohydrate (guarantee reagent, Sinopharm) and 3 g of urea (analytical grade reagents, Sinopharm) were first dissolved in 10 mL of deionized water, and then the transparent solution was dispensed into a 50 mL Teflon-lined stainless steel autoclave which was heated at 180 °C for 4.5 h. After the autoclave being cooled to room temperature, the dark green liquid was collected as N-CQDs.

2.2. Synthesis of N-CQDs/$CaTiO_3$ Composites. The N-CQDs/$CaTiO_3$ was synthesized by dosing predetermined N-CQDs amount into $CaTiO_3$ precursor solution which suffered further solvothermal treatment. In particular, 2 mL of 1 mol/L $Ca(NO_3)_2{\cdot}4H_2O$ (analytical grade reagents, Sinopharm) was dissolved in 37 mL of PEG-200 (polyethylene glycol, chemical purity, Sinopharm), and then 0.7 mL of tetrabutyl titanate [titanium n-butoxide, $Ti(OC_4H_9)_4$, TNB] (chemical pure, Sinopharm) was dosed into this solution being stirred vigorously. A total of 1.76 g of NaOH (chemical purity, Sinopharm) was added into the obtained colloidal solution under continuous stirring as a mineralizer. Subsequently, a predetermined dose of N-CQDs solution was dispensed into the above solution, and the obtained suspension liquid was then relocated to a 50 mL Teflon-lined stainless steel autoclave which was heated at 180 °C for 15 h. After the autoclave was cooled naturally to ambient temperature, the white and yellow samples were collected and washed using dilute acetic acid, deionized water, and ethanol, sequentially. The samples were eventually dried overnight at 60 °C. The N-CQDs/$CaTiO_3$ composites synthesized by varying the N-CQDs solution dose of 0.1, 0.3, and 0.5 mL were labeled as 1-N-CQDs/$CaTiO_3$, 3-N-CQDs/$CaTiO_3$, and 5-N-CQDs/$CaTiO_3$, respectively.

2.3. Characterization. The crystal structure of as-prepared catalysts was analyzed using an X-ray diffractometer (PANalytical X' Pert PRO) with a scan range of 20−80 ° (2θ) at a scan rate of 0.05°/s. Fouriertransform infrared spectroscopy (FT-IR) was conducted on a Magna-IR 750 spectrometer (USA) in the range of 450−2000 cm^{-1}. X-ray photoelectron spectroscopy (XPS; Physical Electrons Quantum2000 Scanning Esca Microprob), scanning electron microscopy (SEM, JEOL JSM-6490), and transmission electron microscopy (TEM, JEOL JEM-2100HRCM-120) were utilized to analyze chemical state, morphology and elemental distribution, and crystalline structure, respectively. The N_2 adsorption/desoption isotherms which can be measured at 77 K with an ASAP 2020 (Micromeritics Instrument Corp, U.S.A.) were recorded in order to determine the BET surface area of the as-synthesized catalysts. Moreover, the reflectance spectra of the catalysts were characterized within a range of 200−800 nm using a Varian Cary 100 Scan UV−vis system.

Themogravimetric analysis (TG) was performed from 25 to 800 °C on a Simultaneous Thermal Analysis instrument (STA 449F5) under nitrogen gas at a flow rate of 30 mL/min. A chemisorption analyzer (BJbuilder, PCA 1200, China) was used for temperature-programmed desorption (TPD): 50 mg of samples was pretreated by N_2 at 300 °C for 30 min with a constant heating rate of 10 °C/min to eliminate surface pollutants. After cooling to room temperature, the catalyst will be exposed in NO for 30 min. Once equilibrated, the sample was placed in the He atmosphere with a heating rate of 10 °C/min to 800 °C to allow desorption of NO. Electron spin resonance spectroscopy (ESR, ER200-SRC, Bruker, Germany) was applied to determine active oxygen species generated during photocatalytic process with 5,5′-dimethyl-1-pirroline-N-oxide (DMPO) solution as an adduct agent. Deionized water and methanol were used as solvents for the identification of DMPO-•OH and DMPO-$•O_2^-$, respectively, under the irradiation of 420 nm visible light. The yield of intermediate and final products such as nitrate and nitrite ions, was quantified by Ion Chromatograph (IC, Dionex-600, U.S.A.) equipped with an IonPac AS14A column.

The photocurrent measurement of as-synthesized samples was similar to our previous studies.[36]

2.4. Photocatalytic Activity Test. The photocatalytic activities of $CaTiO_3$ and N-CQDs/$CaTiO_3$ with different N-CQDs dose were examined in terms of NO removal. The chamber for testing was fabricated with stainless steel and covered by quartz glass in accordance with the ISO 22197-1 standard. A 300 W xenon lamp (microsolar 300, Perfectlight, China) was used to offer the visible light (>420 nm) with UV light being removed. For testing, an aqueous suspension with 0.1 g of catalyst was coated onto a glass dish (diameter = 12 cm) by pretreating at 70 °C for few hours to completely remove the water.

The initial NO concentration was 400 ppb, and the flow rate was 3 L/min. A chemiluminescence NO analyzer (model 42c, Thermo Environmental Instruments Inc., Franklin, MA) was used to measure the concentration of NO with a sampling of 0.7 L/min. The photocatalytic reaction using P25 as a catalyst was also conducted under identical conditions as a comparison.

The removal efficiency (η) of NO was calculated as η (%) = $(1 - C/C_0) \times 100$, where C is the NO residual during NO photocatalytic degradation, ppb, and C_0 is NO initial

DOI: 10.1021/acs.iecr.8b01731
Ind. Eng. Chem. Res. 2018, 57, 10226−10233

concentration (ppb). The NO_2 concentration was simultaneously meausred during the photocatalytic process, and its yield can be obtained by using the equation ΔNO_2 (ppb) = $C - C_0$, in which C represents the NO_2 concentration after reaction (ppb) and the C_0 is NO_2 initial concentration. Finally, we can use the equation NO_2 conversion rate = $\Delta NO_2/(C - C_0)$ in which C represents the initial NO concentration and the C_0 represents the NO concentration after reaction to represent the NO_2 conversion ration in the whole experiment.

3. RESULTS AND DISCUSSION

3.1. Phase Structure and Chemical Compositions. The crystal phase of as-synthesized $CaTiO_3$ and N-CQDs/$CaTiO_3$ composites were characterized via XRD. As shown in Figure 1,

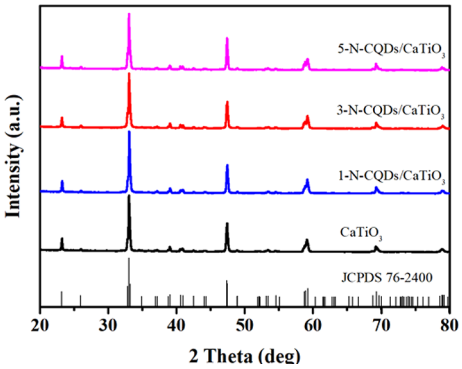

Figure 1. Powder XRD patterns of pure $CaTiO_3$ and N-CQDs nanocomposites with various N-CQDs loading amount.

all diffraction peaks of the tested samples can be ascribed to pure orthorhombic $CaTiO_3$ (a = 5.38290 Å, b = 7.64530 Å, c = 5.44580 Å, JCPDS no. 76-2400). The diffraction peaks at 2θ values of 23.1°, 33.1°, 47.4°, 59.2°, and 69.4° correspond to the (101), (121), (202), (321), and (242) reflections, respectively. However, the characteristic peak of N-CQDs (approximately 25.6°)[37] was not detected in N-CQDs/$CaTiO_3$ composites, which may be on account of the low content and highly scattered N-CQDs in these samples. Moreover, in the case of N-CQDs/$CaTiO_3$ catalysts, no shift of the diffraction peaks of $CaTiO_3$ was observed, indicating that the phase structure of $CaTiO_3$ remained stable in the presence of N-CQDs during the synthesis process.

FT-IR spectra were measured to further confirm the existence of carbon quantum dots in the complex structures of N-CQDs/$CaTiO_3$. As demonstrated in Figure 2a, besides the peaks coming from $CaTiO_3$, a characteristic peak located at 1330 cm^{-1} corresponding to the C−O−C[27] was observed, suggesting the existence of CQDs in the composite catalysts.

To test if the nitrogen was doped into the carbon quantum dots, XPS was conducted over the N-CQDs. As illustrated in Figure 2b, the survey spectrum confirms that the CQDs sample contains N element, indicating nitrogen was successfully doped into the CQDs.

3.2. Morphology. SEM and TEM were utilized to delineate the micrograph and crystallographic structure of the 3-N-CQDs/$CaTiO_3$ material (see Figure 3). As demonstrated in Figure 3a−c, the lattice fringe spacing of 0.383 nm derives from the (101) plane of the orthorhombic-structured $CaTiO_3$, while the lattice fringe spacing of roughly 0.209 nm is attributed to the (010) lattice planes of the hexagonal graphitic carbon.[32]

The SEM images of the 3-N-CQDs/$CaTiO_3$ sample are illustrated in Figure 3d and Figure S1. The cubic particles with a size ranging from 500 nm to 1 μm can be observed. As demonstrated in Figure S1, after being modified by suitable N-CQDs, $CaTiO_3$ maintains the original shape. However, with the addition of 0.5 mL of N-CQDs, the agglomeration can be observed, implying overdose N-CQDs can change the morphology of $CaTiO_3$. With the aim of investigating the elemental dispersion over the N-CQDs/$CaTiO_3$ composite, EDX mapping was recorded and shown in Figure 3e−h. The result suggests that Ca (green), Ti (blue), O (purple), and N (yellow) elements are distributed evenly on the surface of the sample. The sparse presence of N in comparison with other elements provided cogent evidence for the distribution of N-CQDs on the surface of $CaTiO_3$. It can be concluded that N-CQDs/$CaTiO_3$ composite was successfully synthesized.

3.3. Textural, Optical, Electric, and Adsorption Properties of Samples. The specific surface area of $CaTiO_3$ was 13.0 m^2/g, twice that of 3-N-CQDs/$CaTiO_3$ (6.4 m^2/g), indicating the addition of N-CQDs reduced the BET surface area of CQDs (see Table S1). The agglomeration was observed with the introduction of N-CQDs as demonstrated in Figure S1, justifying the reduction of BET surface area of $CaTiO_3$ with the presence of N-CQDs.

In the presence of N-CQDs, the composite's absorption spectra exhibit an apparent red shift, where the absorption edge extends to the visible region (see Figure 4a). Furthermore, such a red shift hinges on the N-CQDs content. Pure $CaTiO_3$ can only absorb UV light (<368 nm), based on

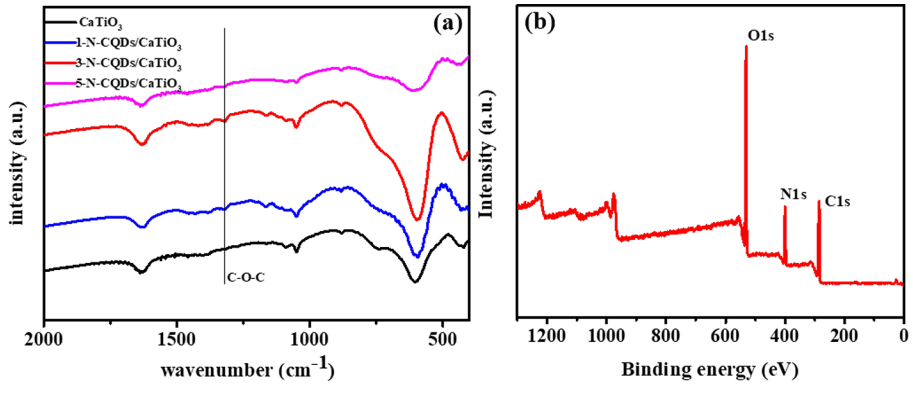

Figure 2. (a) FT-IR spectra of as-prepared samples; (b) survey XPS spectra of N-CQDs.

DOI: 10.1021/acs.iecr.8b01731
Ind. Eng. Chem. Res. 2018, 57, 10226−10233

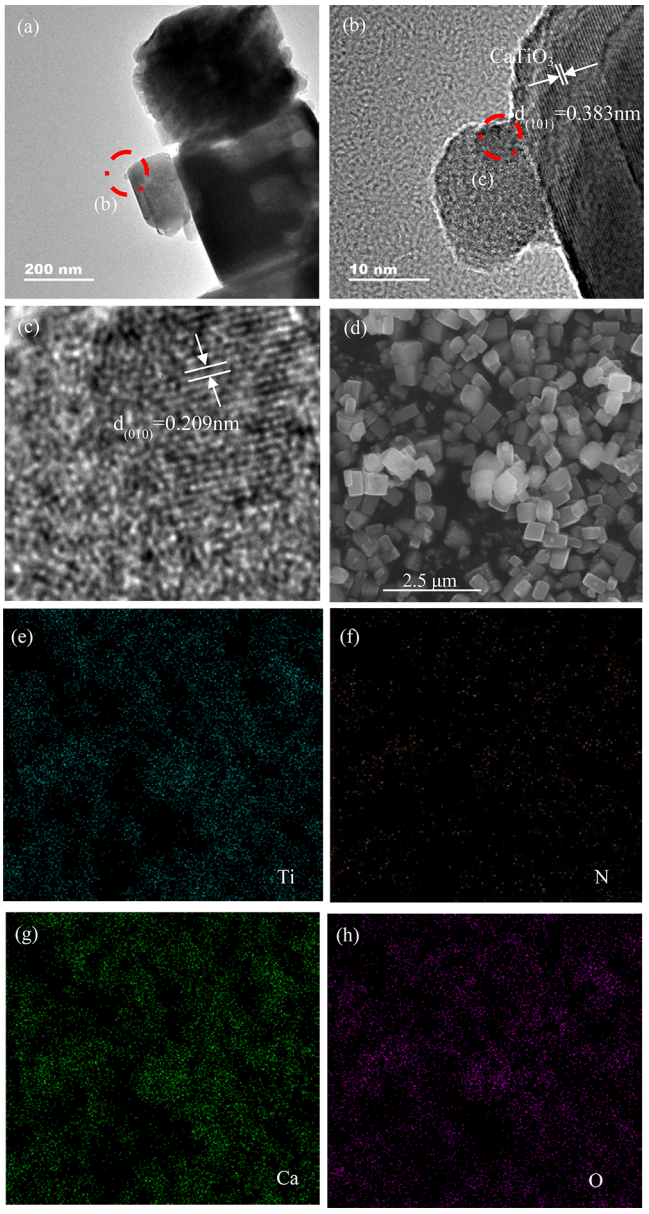

Figure 3. (a–c) HRTEM images of 3-N-CQDs/$CaTiO_3$ and; (d) SEM images of the 3-N-CQDs/$CaTiO_3$; (e–h) representative the EDX mapping images corresponding to (d).

which its band gap can be calculated to be 3.27 eV using the $(\alpha h\nu)^2$ as a function of $h\nu$ (see Figure 4b). This result indicates that the introduction of N-CQDs allows $CaTiO_3$ to be excited under the illumination of visible light (>420 nm). This phenomenon can be rationalized by the up-conversion fluorescence properties of N-CQDs that can emit light at shorter wavelength than the excitation light. Consequently, when visible light was used as the excitation light, it can be converted to UV light so that the $CaTiO_3$ can be excited.[33,38]

Photoelectrochemistry tests were carried out to probe the divorcement of photogenerated carriers. The transitory photocurrent generation over $CaTiO_3$/FTO (fluorine-doped tin oxide) and 3-N-CQDs/$CaTiO_3$/FTO electrodes was detected in Na_2SO_3 solution under recurrent illumination of visible light at a wavelength of 420 nm. As shown in Figure 4c, the photocurrent response of $CaTiO_3$ is extremely weak with the visible light being turned on whereas the photocurrent generated over 3-N-CQDs/$CaTiO_3$ is roughly 2.5 times larger than that over pure $CaTiO_3$. The result implies that N-CQDs are capable of advancing the divorce of photogenerated carriers over $CaTiO_3$ and eventually contribute to the larger photocurrent generation.[25] The electrons captured by O_2 on the surface of the 3-N-CQDs/$CaTiO_3$ and the reunion of electrons and holes resulted in the loss of photocurrent (ΔI) during the irradiation duration of visible light.[39,40] Intriguingly, ΔI weakened during recurrent irradiation of visible light. This is because the amount of adsorbed O_2 on the surface of catalysts decreased with the illumination time due to the limited diffusion of O_2 to the surface of catalysts.

It was also noted that the photocurrent is low even over N-CQDs/$CaTiO_3$. One of the functions of N-CQDs is to promote the divorce of charge carrier in $CaTiO_3$. However, the content of N-CQDs is very low (less than 1%) in N-CQDs/$CaTiO_3$, which may lead to the limited promoting effects of N-CQDs on the separation of charge carrier. On the other hand, up-conversion fluorescence properties of N-CQDs render N-CQDs/$CaTiO_3$ excited by visible light. The weak absorption of visible light by low-content N-CQDs may cause weak emission of UV light for the excitation of $CaTiO_3$, which also rationalize the low photocurrent generated over N-CQDs/$CaTiO_3$ under visible light irradiation.

3.4. Photocatalytic Activity and Reaction Mechanisms. The energy band structure plays a vital role in the activity of photocatalysts. The valence band position is 2.46 eV based on the valence band (VB) XPS of $CaTiO_3$ (see Figure 4d). On the basis of the formula $E_{CB} = E_{VB} - E_g$, and the band gap (E_g) of $CaTiO_3$ (3.27 eV), the conduction band position (E_{CB}) of $CaTiO_3$ was determined to be −0.81 eV. In order to confirm the band position of $CaTiO_3$, ESR spectroscopy was conducted to identify hydroxyl radicals (DMPO-•OH) in $CaTiO_3$ aqueous suspension and superoxide radicals (DMPO-O_2^-) in $CaTiO_3$ methanol suspension under UV irradiation. As shown in the Figure S3, $CaTiO_3$ can produce the $\bullet O_2^-$ and •OH under UV irradiation, suggesting the CB potential negative to the redox potential of $O_2/\bullet O_2^-$(−0.33 eV) and the VB potential positive to the H_2O/•OH (2.37 eV),[41] implying the calculated band positions of $CaTiO_3$ was reasonable in this study. Mizoguchi et al. reported the CB potential was −0.78 eV which was similar to that in our study.[42] It was observed that the addition of PEG could red shift the light absorption of the material so that the band gap was narrowed to the 3.27 eV.[43]

It was reported that the presence of carbonaceous materials promote the adsorption of dye on the TiO_2.[44] To evaluate the influence the introduction of N-CQDs on the adsorption ability of $CaTiO_3$, TGA and NO-TPD were conducted to explore the interaction between NO and the as-synthesized photocatalysts. The TGA curve of samples shows three weight loss stages (see Figure 5a). It is worth noting that, in the third stage above 580 °C, the curve of pure $CaTiO_3$ has no change, and the mass loss of N-CQDs/$CaTiO_3$ linearly correlated with the N-CQDs contents. It can be concluded that N-CQDs are decomposed above 580 °C. It is also intriguing to notice that the whole weight loss of 5-N-CQDs/$CaTiO_3$ is more than 15%, indicating that the addition of 0.5 mL of N-CQDs will change the crystal of $CaTiO_3$ which lead to the difference of photocatalytic activity (see Figure S1). Figure 5b shows that pure $CaTiO_3$ has two discernible desorption peaks: the peak at around 350 °C coming from the desorption of NO (N-CQDs will decomposed above 580 °C) and the one at 630 °C

DOI: 10.1021/acs.iecr.8b01731
Ind. Eng. Chem. Res. 2018, 57, 10226–10233

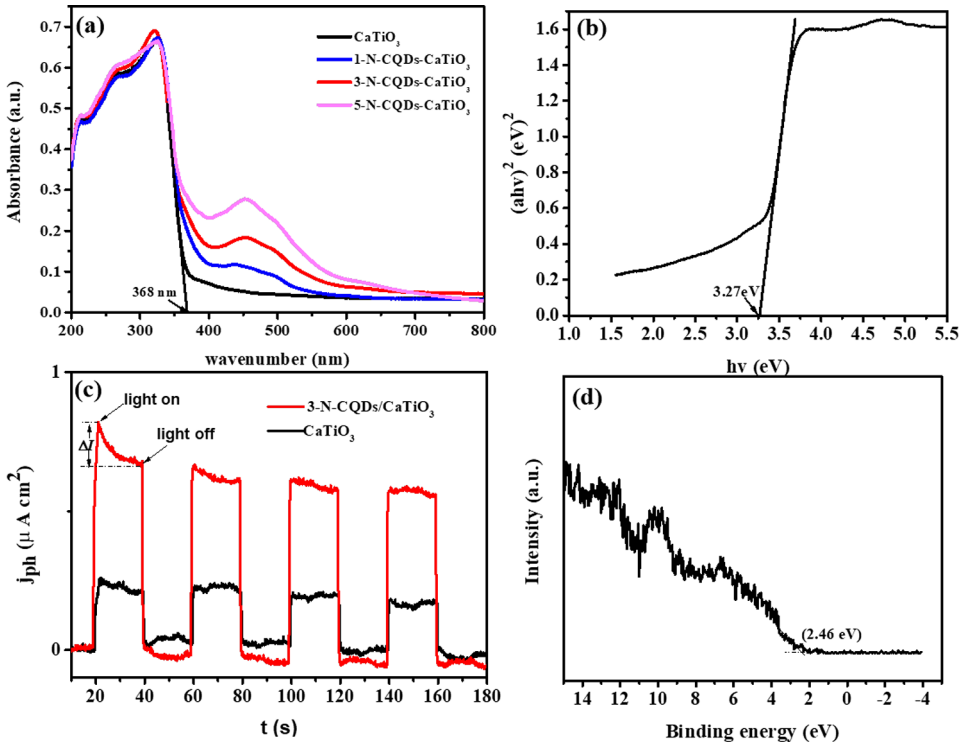

Figure 4. (a) UV−visible diffuse reflectance spectra of $CaTiO_3$ and N-CQDs/$CaTiO_3$; (b) $(\alpha h\nu)^2$ vs $h\nu$ of $CaTiO_3$; (c) photocurrent responses of $CaTiO_3$ and 3-N-CQDs/$CaTiO_3$ in 0.5 M Na_2SO_3 electrolyte under visible light irradiation (λ = 420 nm); (d) valence band XPS spectra of pure $CaTiO_3$.

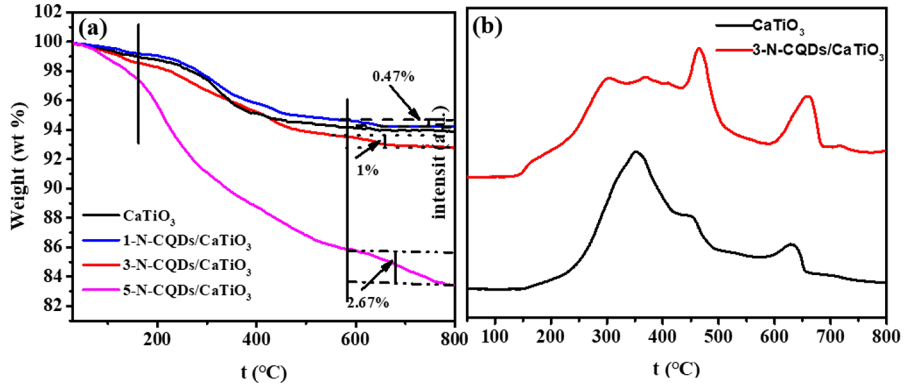

Figure 5. (a) TGA of $CaTiO_3$ and N-CQDs/$CaTiO_3$; (b) TPD profiles of NO for the as-prepared pristine $CaTiO_3$ and 3-N-CQDs/$CaTiO_3$.

deriving from the release of O_2 from the $CaTiO_3$ lattice.[45] This suggests that NO can be chemically adsorbed onto the $CaTiO_3$ surface at ambient temperature. The NO desorption as a function of temperature is also presented over the 3-N-CQDs/$CaTiO_3$. In contrast to $CaTiO_3$, the NO desorption temperature shifted to 450 °C over 3-N-CQDs/$CaTiO_3$, indicating the enhanced adsorption capacity of 3-N-CQDs/$CaTiO_3$. It can be concluded that the N-CQDs may have the potential to increase the adsorption ability of $CaTiO_3$.

Based on the aforementioned results, the introduction of N-CQDs can broaden the optical response range to allow $CaTiO_3$ to be excited by visible light. The intrinsic electron storage capacity of N-CQDs allows the efficient divorcement of the photogenerated carriers. The N-CQDs can enhance the adsorption ability for NO which would fundamentally boost the photocatalytic performances.

The visible light-driven photocatalytic activities of $CaTiO_3$ and N-CQDs/$CaTiO_3$ composites were gauged in terms of the photocatalytic elimination of NO_x. As illustrated in Figure 6a, the NO removal efficiency was enhanced when the N-CQDs dose was escalated. The best performance was achieved over 3-N-CQDs/$CaTiO_3$, where the concentration of nitrogen oxide at the outlet decreased 25% in comparison with that at the inlet removed after 0.5 h. The decrease of NOx concentration is almost 5 times larger than that over $CaTiO_3$ (5%) and apparently larger than that over P25 (14%). No significant deactivation was observed in 30 min. With the further increment of the N-CQDs dose, the photocatalytic activity of 5-N-CQDs/$CaTiO_3$ decreased although 5-N-CQDs/$CaTiO_3$ has the strongest visible light absorption. The higher N-CQDs content made the $CaTiO_3$ agglomerate as shown in Figure S1, leading to less active sites available for NO adsorption. The concentration of NO_2 in the outlet gas was concurrently

DOI: 10.1021/acs.iecr.8b01731
Ind. Eng. Chem. Res. 2018, 57, 10226−10233

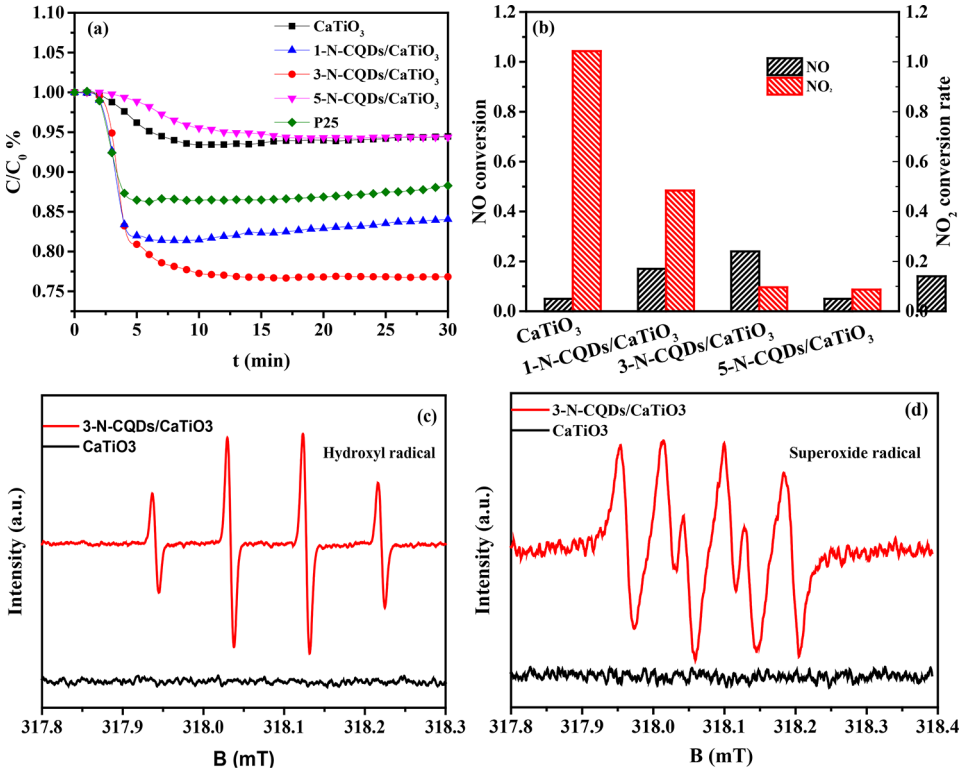

Figure 6. (a) Visible light photocatalytic removal of NO; (b) comparison of the NO conversion rate (C/C_0) and NO_2 conversion rate over $CaTiO_3$, N-CQDs/$CaTiO_3$ and P25; (c and d) DMPO spin-trapping ESR spectra of $CaTiO_3$ and 3-N-CQDs/$CaTiO_3$ in aqueous dispersion for DMPO-•OH and in methanol dispersion for DMPO-$•O_2^-$ under illumination for 12 min ($\lambda \geq 420$ nm).

detected. The NO removal efficiency ($C_0 - C/C_0$) and NO_2 conversion ratio ($\Delta NO_2/(C_0 - C)$) over different samples are presented in Figure 6b. The 3-N-CQDs/$CaTiO_3$ composite shows superior performance in terms of NO_2 yield (9.6%), which is lower than that over pure $CaTiO_3$ (104.3%) .

The stability of the 3-N-CQDs/$CaTiO_3$ composite was examined by the repeated photocatalytic experiments under identical conditions (see Figure S2). The NO removal efficiency decreased to 16% after 3-N-CQDs/$CaTiO_3$ being recycled for 5 times, implying that the catalyst is relatively unstable. However, being washed by deionized water can restore the photocatalytic activity of 3-N-CQDs/$CaTiO_3$, which can be rationalized by the elimination of NO oxidation products including NO_3^- and NO_2^- on the catalyst surface. The concentration of nitrate and nitrite ions on the surface of $CaTiO_3$ and 3-N-CQDs/$CaTiO_3$ after single run reaction was detected and shown in Table S1. NO_3^- generated on 3-N-CQDs/$CaTiO_3$ surfaces was quantified to be 57.28 $\mu g/m^2$, which is 1.46 times as high as that generated on the $CaTiO_3$ (39.29 $\mu g/m^2$), implying that the presence of N-CQDs shifted the photocatalytic reaction on the $CaTiO_3$ surface toward the yield of nitrate formation. Besides, the generation of trace NO_2^- was observed.

ESR spectroscopy was conducted to determine the reactive radicals participating in photocatalytic oxidation of NO over $CaTiO_3$ and 3-N-CQDs/$CaTiO_3$ under visible light illumination. Figure 6c,d shows no signal in the case of $CaTiO_3$, indicating that neither $•O_2^-$ nor •OH radicals were generated. Both the typical DMPO-$•O_2^-$ and DMPO-•OH signals were strong in the case of the 3-N-CQDs/$CaTiO_3$ sample.

The photocatalytic reaction process for the NO degradation over the N-CQDs/$CaTiO_3$ composite is described in Figure 7.

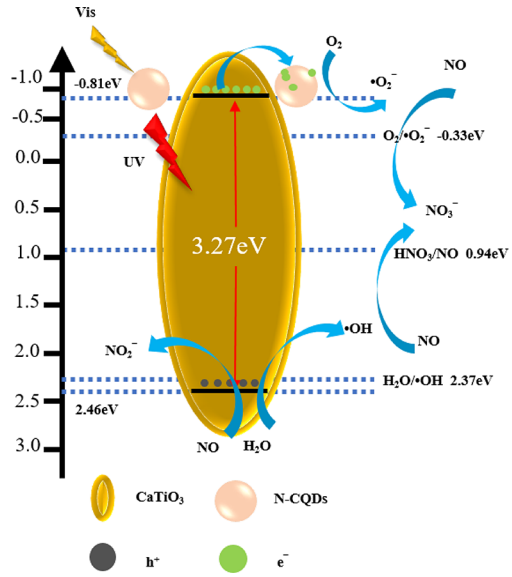

Figure 7. Proposed photocatalytic mechanism for enhancing photocatalytic activity over the 3-N-CQDs/$CaTiO_3$ composite under visible light irradiation.

Under the irradiation of visible light, the N-CQDs adsorb visible light and then radiate UV light owing to up-conversion effects, which in turn excite $CaTiO_3$ to spawn electron and hole pairs. The carbon nanomaterials have the potential to accept and transport electrons, which favored the electrons being transferred from CB of $CaTiO_3$ to N-CQDs and accumulating on the N-CQDs. As a result, electrons-holes pairs were separated efficiently. In addition, the introduction of N-

DOI: 10.1021/acs.iecr.8b01731
Ind. Eng. Chem. Res. 2018, 57, 10226−10233

CQDs promoted NO adsorption over $CaTiO_3$, which is also beneficial for the oxidation reaction of NO.

The whole process of photocatalytic NO removal over the N-CQDs/$CaTiO_3$ composite under visible light is described as the following:

$$CaTiO_3 + N - CQDs + vis \rightarrow e^- + h^+ \quad (1)$$

$$h^+ + NO + H_2O \rightarrow NO_2^- + 2H^+ \quad (2)$$

$$e^- + O_2 \rightarrow \bullet O_2^- \quad (3)$$

$$\bullet O_2^- + 2H^+ + 2e^- \rightarrow \bullet OH + OH^- \quad (4)$$

$$NO_x + \bullet O_2^- \rightarrow NO_3^- \quad (5)$$

$$2 \bullet OH + NO \rightarrow NO_2 + H_2O \quad (6)$$

$$NO_2 + \bullet OH \rightarrow NO_3^- + H^+ \quad (7)$$

4. CONCLUSIONS

In brief, a facile hydrothermal method was used to construct a N-CQDs/$CaTiO_3$ composite photocatalyst. In contrast with $CaTiO_3$ and P25, the composite exhibits increased visible light-induced photocatalytic activity with respect to NO degradation and lower selectivity toward NO_2 formation. The N-CQDs are believed to play multiple roles including wavelength converter, electron reservoir, and transporter as well as an excellent NO_x adsorber during the photocatalytic oxidation of NO over N-CQDs/$CaTiO_3$; the synergistic effects of these multiple roles account for the superior photocatalytic capacity of N-CQDs/$CaTiO_3$.

■ ASSOCIATED CONTENT

Supporting Information

The Supporting Information is available free of charge on the ACS Publications website at DOI: 10.1021/acs.iecr.8b01731.

Figure for SEM images of every catalysts, figure for the cyclic NO degradation tests, figure for DMPO spin-trapping ESR spectra of $CaTiO_3$ under UV light illumination, table for the BET specific surface area, and the amount of nitrate and nitrite accumulated on the surface of $CaTiO_3$ and 3-N-CQDs/$CaTiO_3$ (PDF)

■ AUTHOR INFORMATION

Corresponding Authors

*E-mail: yfrao@mail.xjtu.edu.cn.
*E-mail: huangyu@ieecas.cn.

ORCID

Yongfang Rao: 0000-0002-3265-4151
Yu Huang: 0000-0003-3334-4849

Notes

The authors declare no competing financial interest.

■ ACKNOWLEDGMENTS

This work was financially supported by "State Key Laboratory of Loess and Quaternary Geology, Institute of Earth Environment, CAS (No. SKLLQG1516)" and "Key Laboratory of Aerosol Chemistry and Physics, Institute of Earth Environment, CAS (No. KLACP1701)".

■ REFERENCES

(1) Zhao, B.; Wang, S. X.; Liu, H.; Xu, J. Y.; Fu, K.; Klimont, Z.; Hao, J. M.; He, K. B.; Cofala, J.; Amann, M. NO_x emissions in China: historical trends and future perspectives. *Atmos. Chem. Phys.* **2013**, *13* (19), 9869−9897.

(2) Bilgen, S. Structure and environmental impact of global energy consumption. *Renewable Sustainable Energy Rev.* **2014**, *38*, 890−902.

(3) Zhao, B.; Liou, K. N.; Gu, Y.; Li, Q. B.; Jiang, J. H.; Su, H.; He, C. L.; Tseng, H. L. R.; Wang, S. X.; Liu, R.; Qi, L.; Lee, W. L.; Hao, J. M. Enhanced PM2.5 pollution in China due to aerosol-cloud interactions. *Sci. Rep.* **2017**, *7*, 1−11.

(4) Huang, R. J.; Zhang, Y.; Bozzetti, C.; Ho, K. F.; Cao, J. J.; Han, Y.; Daellenbach, K. R.; Slowik, J. G.; Platt, S. M.; Canonaco, F. High secondary aerosol contribution to particulate pollution during haze events in China. *Nature* **2014**, *514* (7521), 218−222.

(5) Quan, J. N.; Liu, Q.; Li, X.; Gao, Y.; Jia, X. C.; Sheng, J. J.; Liu, Y. G. Effect of heterogeneous aqueous reactions on the secondary formation of inorganic aerosols during haze events. *Atmos. Environ.* **2015**, *122*, 306−312.

(6) Song, C. B.; Wu, L.; Xie, Y. C.; He, J. J.; Chen, X.; Wang, T.; Lin, Y. C.; Jin, T. S.; Wang, A. X.; Liu, Y.; Dai, Q. L.; Liu, B. S.; Wang, Y. N.; Mao, H. J. Air pollution in China: Status and spatiotemporal variations. *Environ. Pollut.* **2017**, *227*, 334−347.

(7) Granger, P.; Parvulescu, V. I. Catalytic NO(x) abatement systems for mobile sources: from three-way to lean burn after-treatment technologies. *Chem. Rev.* **2011**, *111* (5), 3155−3207.

(8) Macleod, N.; Cropley, R.; Keel, J. M.; Lambert, R. M. Exploiting the synergy of titania and alumina in lean NO $_x$ reduction: in situ ammonia generation during the Pd/TiO_2 $/Al_2O_3$ − catalysed H_2 $/CO/NO/O_2$ reaction. *J. Catal.* **2004**, *221* (1), 20−31.

(9) Tanaka, T.; Teramura, K.; Arakaki, K.; Funabiki, T. Photo-assisted NO reduction with NH_3 over TiO_2 photocatalyst. *Chem. Commun.* **2002**, *22* (22), 2742−2743.

(10) Schneider, J.; Matsuoka, M.; Takeuchi, M.; Zhang, J.; Horiuchi, Y.; Anpo, M.; Bahnemann, D. W. Understanding TiO_2 photocatalysis: mechanisms and materials. *Chem. Rev.* **2014**, *114* (19), 9919−9986.

(11) Hoffmann, M. R.; Martin, S. T.; Choi, W.; Bahnemann, D. W. Environmental Applications of Semiconductor Photocatalysis. *Chem. Rev.* **1995**, *95* (1), 69−96.

(12) Boyjoo, Y.; Sun, H.; Liu, J.; Pareek, V. K.; Wang, S. A review on photocatalysis for air treatment: From catalyst development to reactor design. *Chem. Eng. J.* **2017**, *310*, 537−559.

(13) Tanaka, H.; Misono, M. Advances in designing perovskite catalysts. *Curr. Opin. Solid State Mater. Sci.* **2001**, *5* (5), 381−387.

(14) Zhu, J.; Thomas, A. Perovskite-type mixed oxides as catalytic material for NO removal. *Appl. Catal., B* **2009**, *92* (3−4), 225−233.

(15) Zhang, Q.; Huang, Y.; Xu, L.; Cao, J.-j.; Ho, W.; Lee, S. C. Visible-Light-Active Plasmonic Ag-SrTiO3 Nanocomposites for the Degradation of NO in Air with High Selectivity. *ACS Appl. Mater. Interfaces* **2016**, *8* (6), 4165−4174.

(16) Grabowska, E. Selected perovskite oxides: Characterization, preparation and photocatalytic properties-A review. *Appl. Catal., B* **2016**, *186*, 97−126.

(17) Alammar, T.; Hamm, I.; Wark, M.; Mudring, A. V. Low-temperature route to metal titanate perovskite nanoparticles for photocatalytic applications. *Appl. Catal., B* **2015**, *178*, 20−28.

(18) Lozano-Sánchez, L. M.; Méndez-Medrano, M. G.; Colbeau-Justin, C.; Rodríguez-López, J. L.; Hernández-Uresti, D. B.; Obregón, S. Long-lived photoinduced charge-carriers in Er^{3+} doped $CaTiO_3$ for photocatalytic H_2 production under UV irradiation. *Catal. Commun.* **2016**, *84*, 36−39.

(19) Han, C.; Liu, J.; Yang, W.; Wu, Q.; Yang, H.; Xue, X. Photocatalytic activity of $CaTiO_3$ synthesized by solid state, sol-gel and hydrothermal methods. *J. Sol-Gel Sci. Technol.* **2017**, *81* (3), 806−813.

(20) Huang, X.-j.; Yan, X.; Wu, H.-y.; Fang, Y.; Min, Y.-h.; Li, W.-s.; Wang, S.-y.; Wu, Z.-j. Preparation of Zr-doped $CaTiO_3$ with enhanced charge separation efficiency and photocatalytic activity. *Trans. Nonferrous Met. Soc. China* **2016**, *26* (2), 464−471.

DOI: 10.1021/acs.iecr.8b01731
Ind. Eng. Chem. Res. 2018, 57, 10226−10233

(21) Han, C.; Liu, J.; Yang, W.; Wu, Q.; Yang, H.; Xue, X. Enhancement of photocatalytic activity of $CaTiO_3$ through HNO_3 acidification. *J. Photochem. Photobiol., A* **2016**, *322*−*323*, 1−9.
(22) Nishimoto, S.; Matsuda, M.; Miyake, M. Photocatalytic activities of rh-doped $CaTiO_3$ under visible light irradiation. *Chem. Lett.* **2006**, *35* (3), 308−309.
(23) Lim, S. Y.; Shen, W.; Gao, Z. Carbon quantum dots and their applications. *Chem. Soc. Rev.* **2015**, *44* (1), 362−381.
(24) Duo, F.; Wang, Y.; Fan, C.; Zhang, X.; Wang, Y. Enhanced visible light photocatalytic activity and stability of CQDs/BiOBr composites: The upconversion effect of CQDs. *J. Alloys Compd.* **2016**, *685*, 34−41.
(25) Huang, Y.; Liang, Y.; Rao, Y.; Zhu, D.; Cao, J. J.; Shen, Z.; Ho, W.; Lee, S. C. Environment-Friendly Carbon Quantum Dots/$ZnFe_2O_4$ Photocatalysts: Characterization, Biocompatibility, and Mechanisms for NO Removal. *Environ. Sci. Technol.* **2017**, *51* (5), 2924−2933.
(26) Ji, M.; Xia, J.; Di, J.; Wang, B.; Yin, S.; Xu, L.; Zhao, J.; Li, H. Ionic Liquid-Assisted Bidirectional Regulation Strategy for Carbon Quantum Dots (CQDs)/$Bi_4O_5I_2$ Nanomaterials and Enhanced Photocatalytic Properties. *J. Colloid Interface Sci.* **2016**, *478*, 324−333.
(27) Zhang, H.; Huang, H.; Ming, H.; Li, H.; Zhang, L.; Liu, Y.; Kang, Z. Carbon quantum dots/Ag_3PO_4 complex photocatalysts with enhanced photocatalytic activity and stability under visible light. *J. Mater. Chem.* **2012**, *22* (21), 10501−10506.
(28) Zhang, P.; Song, T.; Wang, T.; Zeng, H. In-situ synthesis of Cu nanoparticles hybridized with carbon quantum dots as a broad spectrum photocatalyst for improvement of photocatalytic H_2 evolution. *Appl. Catal., B* **2017**, *206*, 328−335.
(29) Zhang, Y.; Jing, N.; Zhang, J.; Wang, Y. Hydrothermal synthesis of nitrogen-doped carbon dots as a sensitive fluorescent probe for the rapid, selective determination of Hg^{2+}. *Int. J. Environ. Anal. Chem.* **2017**, *97* (9), 841−853.
(30) Sopha, H.; Krbal, M.; Ng, S.; Prikryl, J.; Zazpe, R.; Yam, F. K.; Macak, J. M. Highly efficient photoelectrochemical and photocatalytic anodic TiO_2 nanotube layers with additional TiO_2 coating. *Applied Materials Today* **2017**, *9*, 104−110.
(31) Zhang, Y.-Q.; Ma, D.-K.; Zhang, Y.-G.; Chen, W.; Huang, S.-M. N-doped carbon quantum dots for TiO_2-based photocatalysts and dye-sensitized solar cells. *Nano Energy* **2013**, *2* (5), 545−552.
(32) Martins, N. C. T.; Ângelo, J.; Girão, A. V.; Trindade, T.; Andrade, L.; Mendes, A. N-doped carbon quantum dots/TiO_2 composite with improved photocatalytic activity. *Appl. Catal., B* **2016**, *193*, 67−74.
(33) Zhang, Y.; Park, M.; Kim, H. Y.; Ding, B.; Park, S. J. A facile ultrasonic-assisted fabrication of nitrogen-doped carbon dots/BiOBr up-conversion nanocomposites for visible light photocatalytic enhancements. *Sci. Rep.* **2017**, *7*, 1−12.
(34) Wang, F.; Chen, P.; Feng, Y.; Xie, Z.; Liu, Y.; Su, Y.; Zhang, Q.; Wang, Y.; Yao, K.; Lv, W.; Liu, G. Facile synthesis of N-doped carbon dots/g-C_3N_4 photocatalyst with enhanced visible-light photocatalytic activity for the degradation of indomethacin. *Appl. Catal., B* **2017**, *207*, 103−113.
(35) Wei, J.; Li, X.-D.; Wang, H.-Z.; Zhang, Q.-H.; Li, Y.-G. Nitrogen Doped Carbon Quantum Dots/Titanium Dioxide Composites for Hydrogen Evolution under Sunlight. *Wuji Cailiao Xuebao* **2015**, *30* (9), 925−930.
(36) Gao, Y.; Huang, Y.; Li, Y.; Zhang, Q.; et al. Plasmonic Bi/$ZnWO_4$ Microspheres with Improved Photocatalytic Activity on NO Removal under Visible Light. *ACS Sustainable Chem. Eng.* **2016**, *4* (12), 6912−6920.
(37) Chen, Q.; Wang, Y.; Wang, Y.; Zhang, X.; Duan, D.; Fan, C. Nitrogen-doped carbon quantum dots/Ag_3PO_4 complex photocatalysts with enhanced visible light driven photocatalytic activity and stability. *J. Colloid Interface Sci.* **2017**, *491*, 238−245.
(38) Wang, H.; Sun, P.; Cong, S.; Wu, J.; Gao, L.; Wang, Y.; Dai, X.; Yi, Q.; Zou, G. Nitrogen-Doped Carbon Dots for "green" Quantum Dot Solar Cells. *Nanoscale Res. Lett.* **2016**, *11*, 27−32.
(39) Yen, Y. C.; Lin, C. C.; Chen, P. Y.; Ko, W. Y.; Tien, T. R.; Lin, K. J. Green synthesis of carbon quantum dots embedded onto titanium dioxide nanowires for enhancing photocurrent. *R. Soc. Open Sci.* **2017**, *4* (5), 161051.
(40) Yang, D.; Feng, J.; Jiang, L.; Wu, X.; Sheng, L.; Jiang, Y.; Wei, T.; Fan, Z. Photocatalyst Interface Engineering: Spatially Confined Growth of $ZnFe_2O_4$ within Graphene Networks as Excellent Visible-Light-Driven Photocatalysts. *Adv. Funct. Mater.* **2015**, *25* (45), 7080−7087.
(41) Wang, Z.; Huang, Y.; Ho, W.; Cao, J.; Shen, Z.; Lee, S. C. Fabrication of $Bi_2O_2CO_3$ /g-C_3N_4 heterojunctions for efficiently photocatalytic NO in air removal: In-situ self-sacrificial synthesis, characterizations and mechanistic study. *Appl. Catal., B* **2016**, *199*, 123−133.
(42) Mizoguchi, H.; Ueda, K.; Orita, M.; Moon, S. C.; Kajihara, K.; Hirano, M.; Hosono, H. Decomposition of water by a $CaTiO_3$ photocatalyst under UV light irradiation. *Mater. Res. Bull.* **2002**, *37* (15), 2401−2406.
(43) Luevano-Hipolito, E.; Martinez-de la Cruz, A.; Yu, Q. L.; Brouwers, H. J. H. Precipitation synthesis of WO_3 for NOx using PEG as template. *Ceram. Int.* **2014**, *40* (8), 12123−12128.
(44) Pu, S.; Zhu, R.; Ma, H.; Deng, D.; Pei, X.; Qi, F.; Chu, W. Facile in-situ design strategy to disperse TiO_2 nanoparticles on graphene for the enhanced photocatalytic degradation of rhodamine 6G. *Appl. Catal., B* **2017**, *218*, 208−219.
(45) Zhang, Q.; Huang, Y.; Peng, S.; Zhang, Y.; Shen, Z.; Cao, J.-j.; Ho, W.; Lee, S. C.; Pui, D. Y. H. Perovskite $LaFeO_3$ -$SrTiO_3$ composite for synergistically enhanced NO removal under visible light excitation. *Appl. Catal., B* **2017**, *204*, 346−357.

DOI: 10.1021/acs.iecr.8b01731
Ind. Eng. Chem. Res. 2018, 57, 10226−10233